National University of Science and Technology "POLITEHNICA" Bucharest
University Center of Pitesti
Faculty of Mechanics and Technology

SCIENTIFIC BULLETIN
AUTOMOTIVE series
year XXX, no. 34

Experimental and numerical analysis and validation of S460 steel

Mihai ŞTIROSU[1,2], Ştefan TABACU[1]*
[1]National University of Science and Technology POLITEHNICA Bucharest, Pitesti University Center, Faculty of Mechanics and Technology, str. Târgul din Vale Street,110040 Pitesti, Romania
[2]AKA Automotiv SRL, Calinesti, 117207, Arges
*Corresponding author e-mail: stefan.tabacu@upb.ro

Article history
Received 12.05.2024
Accepted 22.07.2024

DOI https://doi.org/10.26825/bup.ar.2024.009

Abstract. Finite elements simulation benefit from a considerable decrease in the associated expenses with an optimal design of components. Numerical models are an efficient tool for performance evaluation, monitoring of structures, damage detection, prediction of service life, and identification of optimal maintenance methods. The success of these numerical predictions is dependent on the quality of the constitutive model adopted for material. When assessing the ultimate resistance of components as fracture as a failure mode, the use of cumulative damage models is required to provide reliable results.
Keywords: S460, material model, finite elements, damage

INTRODUCTION

Finite element simulation of mechanical processes plays a crucial role in engineering. From the economic point of view, finite elements simulation benefit from a considerable decrease in the associated expenses with an optimal design of components. Numerical models are an efficient tool for performance evaluation, monitoring of structures, damage detection, prediction of service life, and identification of optimal maintenance methods. Numerical tools are useful to achieve increased understanding of the physical mechanisms controlling the strength, the ductility and the failure mode of threaded assemblies [1]. The advance of current numerical modelling tools and methods determines the need for numerical models to meet the requirements related to the accuracy and reliability of the results [2].

The use of simple design and evaluation procedures is not capable of capturing at a full scale the performance of many structures [3].

The success of these numerical predictions is dependent on the quality of the constitutive model adopted, including the identification of the material parameters. Thus, numerical simulations require knowledge of the material behavior. Therefore, the constitutive equations implemented in the numerical model must be able to reproduce the material behavior.

Properties such as ultimate strength, inelastic behavior and response, and load distribution characteristics are difficult to predict using conventional models [4]. When assessing the ultimate resistance of components as fracture as a failure mode, the use of cumulative damage models is prescribed [5] [6] [7].

To predict these behaviors, the use of extensive analytical methods or experimental trials are required, which in many cases are not sufficient, economical or expedient, thus as a result, the potential of numerical simulation to predict the performance of most structures increased.

The paper details the experimental and numerical procedures performed for the determination of the mechanical properties of S460 material [8]. The input data for the material model is determined from the experimental inputs.

EXPERIMENTAL WORK

Sample preparation

The dimensions of the sheet-type specimen, according to ASTM E8/E8M - Standard Test Method for Tension Testing of Metallic Materials [9], are shown in Figure 1.

Figure 1. Specimen (ASTM E8/E8M)

Several samples were cut from the blank sheets using a laser. The rolling direction of the blank was not provided. Information relating to the cutting method used is not available.

Therefore, the samples were positioned on the blank sheet according to the pattern [10] presented in Figure 2*a*.

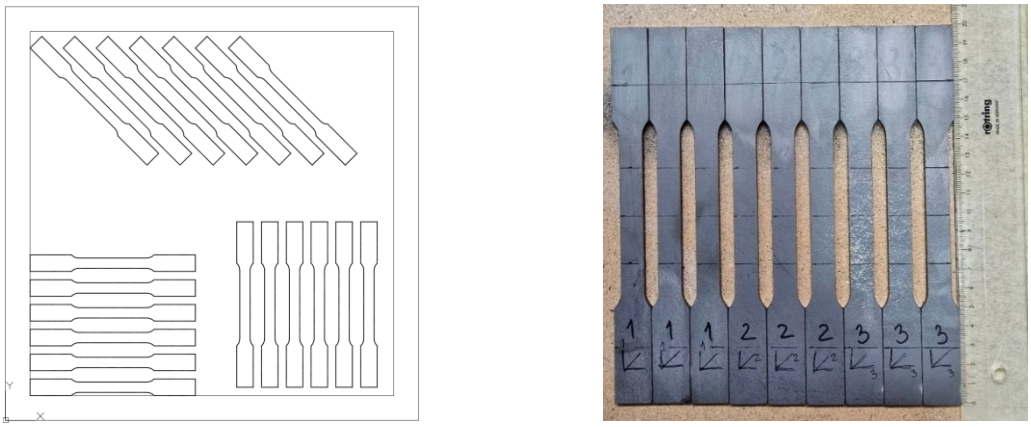

a) *b)*

Figure 2. Cutting pattern for the specimen: *a)* cutting pattern; *b)* specimens

The samples were subsequently numbered according to the orientation (Figure 2*b*). For further reference, direction one indicates horizontal, direction two indicates vertical, and direction three indicates 45° oriented [11].

On each specimen, the calibrated region (gauge) and the clamping ends were constructed.

Testing Equipment

The tests were performed on a Universal Testing Machine (electromechanical type) of Class 0.5.

The configuration of the testing method is presented in Figure 4.

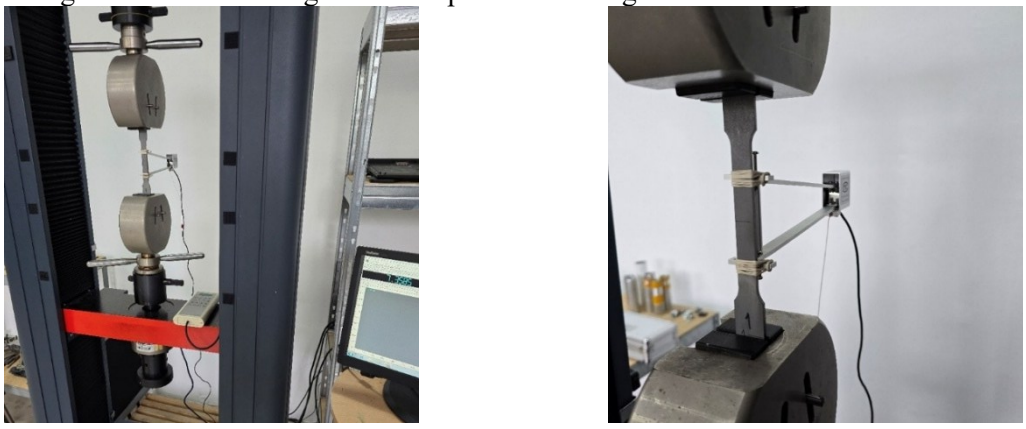

a) *b)*

Figure 3. Universal Testing Machine: *a)* general view; *b)* mechanical extensometer

The machine (Figure 4*a*) is fitted with a 50 kN load cell and can develop a speed of 0.001 to 500 mm/min.

A mechanical extensometer (Figure *4b*) was mounted on each specimen to get an accurate reading of the displacement.

The measurements were performed using the predefined loading procedure provided by the software tool.

EXPERIMENTAL RESULTS

The results obtained from the experimental test are presented in Figure 1.

Direction	Specimen	R_p $[MPa]$	$R_m[MPa]$
1	1	466	539
	2	466	535
	3	471	540
2	1	467	528
	2	469	528
	3	469	530
3	1	481	547
	2	482	546
	3	480	545

Reference values:

$$\boldsymbol{R_p > 460\ MPa}$$
$$\boldsymbol{R_p \in [540 \ldots 720]\ MPa}$$

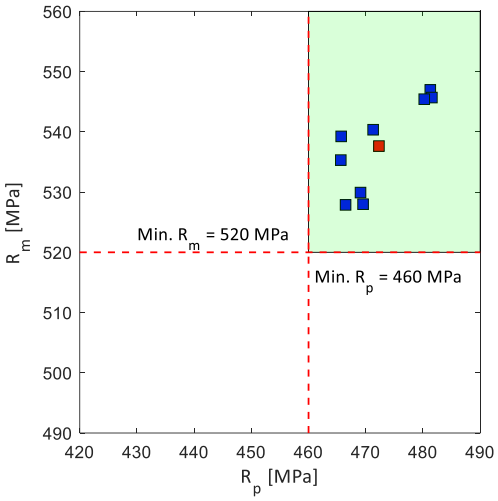

Figure 4. $R_m$vs. R_p- all samples

Stress strain data for each batch are presented in Figure 5.

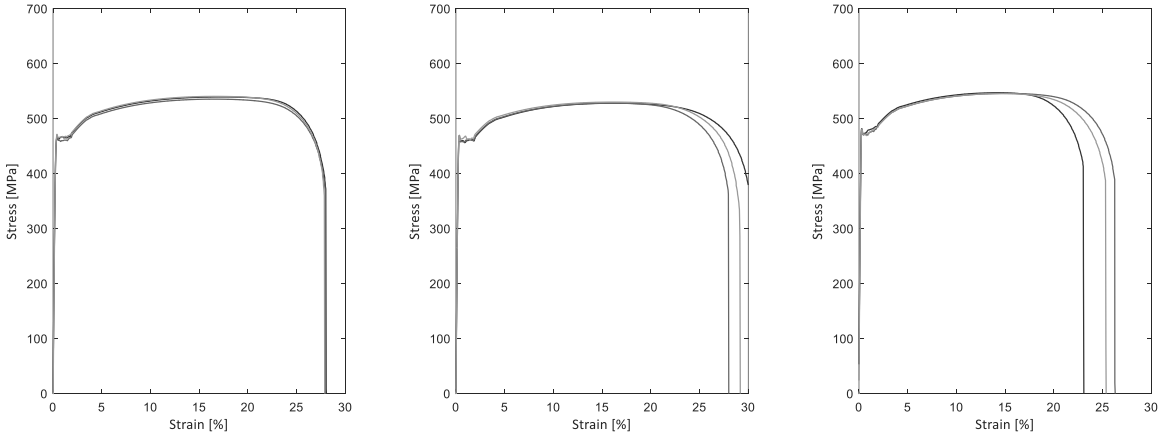

Averaged values:
$R_{p,a} = 467\ MPa$
$R_{m,a} = 538\ MPa$
a)

Averaged values:
$R_{p,a} = 468\ MPa$
$R_{m,a} = 529\ MPa$
b)

Averaged values:
$R_{p,a} = 481\ MPa$
$R_{m,a} = 546\ MPa$
d)

Figure 5. Stress–strain curves: *a)* direction one; *b)* direction two; *c)* direction three

Results listed in Table 1 and displayed in Figure 5 reveal that the specimens in direction three present a slightly increased value for the yield stress (+4.5%) and the maximum stress (+3.2%). However, the differences do not justify the identification of a priority direction for workpiece extraction from the blank.

True stress-strain

The data listed in Section 4 refers to the measurement. To develop a correct material model for analytical and numerical analyses, true stress and strain data are required [12] [13].

Equation 1 provides engineering to true stress and strain.

$$\begin{aligned} \varepsilon_t &= \log(1 + \varepsilon_e) \\ \sigma_t &= \sigma_e \cdot (1 + \varepsilon_e) \end{aligned} \tag{1}$$

ε_e and σ_e are the recorded data;

ε_t and σ_t are the corrected data;

The strain is measured by the extensometer considering the change in length of the gauge $(L - L_0)$ over the initial length of the gauge (L_0)

$$\varepsilon_e = \frac{L - L_0}{L_0} \tag{2}$$

The stress is measured from the force (F) recorded by the load cell divided by the area of the cross – section (A_0).

$$\sigma_e = \frac{F}{A_0} \tag{3}$$

The datasets are limited to the interval $[0 \dots \varepsilon_m]$, where ε_m is the strain corresponding to the maximum stress (R_m).

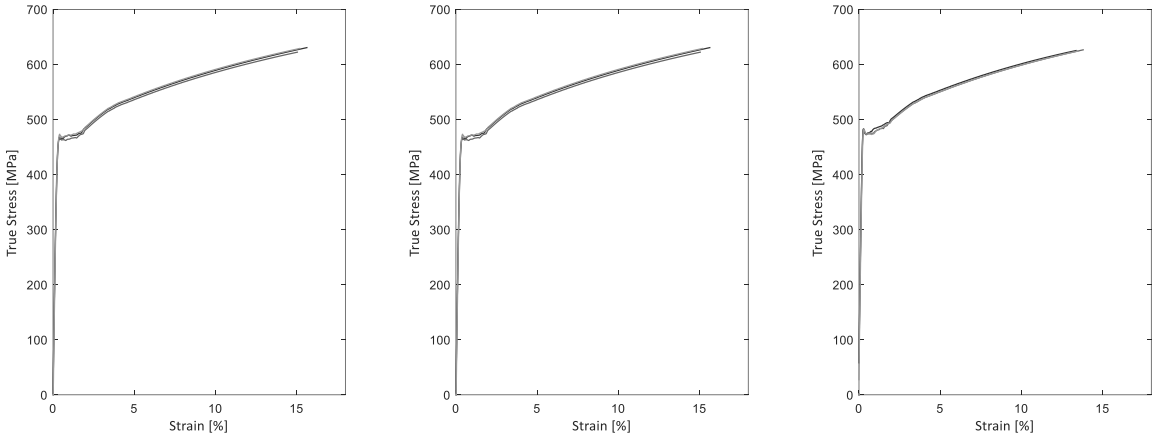

Averaged values:
$\varepsilon_{m,a} = 0.15$
$\sigma_{m,a} = 627\ MPa$
a)

Averaged values:
$\varepsilon_{m,a} = 0.15$
$\sigma_{m,a} = 615\ MPa$
b)

Averaged values:
$\varepsilon_{m,a} = 0.14\ MPa$
$\sigma_{m,a} = 625\ MPa$
c)

Figure 6. True stress–strain curves: *a)* direction one; *b)* direction two; *c)* direction three

NUMERICAL VALIDATION

Results obtained for the true stress – strain curves are used to define the material card for the numerical simulation.

Material *MAT_PIECEWISE_LINEAR_PLASTICITY is implemented for the numerical simulation [14] [15].

A numerical model of a specimen according to dimensions presented in Figure 1 was developed. Figure 7 presents the configuration of the model.

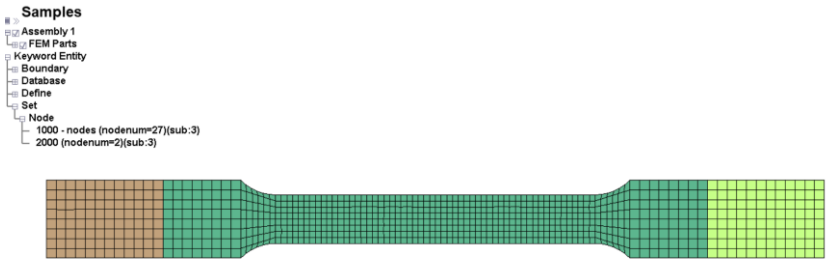

Figure 7. Numerical model

The middle section is the deformable section of the specimen. The material associated with this section is *MAT_PIECEWISE_LINEAR_PLASTICITY.

The left section defines the fixed end of the specimen. The right section is the mobile end of the specimen associated with the mobile part of the testing machine. The material associated with these sections is *MAT_RIGID. Several nodes on the cross-section are defined to measure the reaction force (Figure 8).

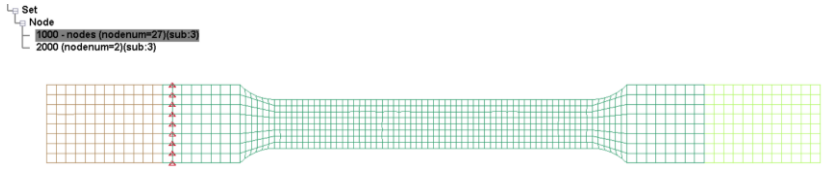

Figure 8. Nodes for force measurement

A pair of nodes define the extensometer for strain measurement (Figure 9).

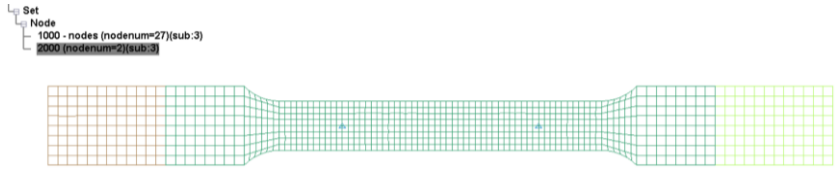

Figure 9. Nodes for strain measurement

The numerical model is solved using the implicit solver with the parameters used for the common applications.

Numerical vs. experimental data are presented in Figure 10.

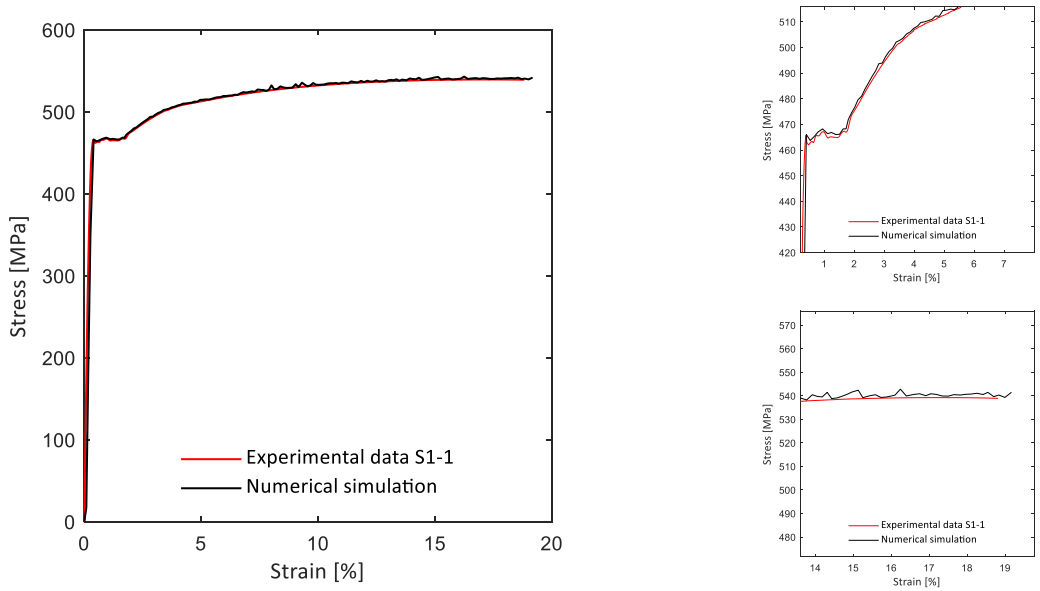

Figure 10. Numerical vs. experimental data

Results presented in Figure 10 show a very good agreement of the numerical results with the experimental data.

The softening behavior of the material under a tensile load is a consequence of a void development in the part and a change in the cross-section and this requires correction in the stress-strain curve in order to obtain reliable input data for numerical analysis. The difference between the updated stress and the true calculated stress is compensated by using a damage parameter. In Ls-Dyna, the mechanism for failure is based on the use of the *MAT_ADD_DAMAGE_GISSMO card. The GISSMO model – *generalized incremental stress-state dependent damage model* – [16,17] [18] is based on the use of triaxiality measure where the triaxiality is the measure of the ratio of the hydrostatic mean stress (σ_h) to the equivalent von Mises stress ($\bar{\sigma}$), and provides a solution to define the loading states [19] [20].

$$\eta = \frac{\sigma_h}{\bar{\sigma}} \tag{4}$$

where σ_h is the mean stress or the hydrostatic pressure and $\bar{\sigma}$ is the equivalent or von Mises stress. These terms are defined in terms of the principal stresses ($\sigma_1, \sigma_2, \sigma_3$), by:

$$\sigma_h = \frac{1}{3} \cdot (\sigma_1 + \sigma_2 + \sigma_2) \tag{5}$$

and:

$$\bar{\sigma} = \frac{1}{3} \cdot \sqrt{\frac{(\sigma_1 - \sigma_2)^2 + (\sigma_2 - \sigma_3)^2 + (\sigma_3 - \sigma_1)^2}{2}} \tag{6}$$

The GISSMO model is based on the incremental formulation of the damage accumulation in the form of:

$$\Delta D = \frac{\varepsilon}{\varepsilon_f(\eta)} \cdot D^{(1-1/\mathrm{DMGEXP})} \cdot \Delta\varepsilon \tag{7}$$

where $\varepsilon_f(\eta)$ is the equivalent plastic strain to failure determined from the input curve (as a function of the triaxiality parameter), $\Delta\varepsilon$ is the equivalent plastic strain increment, and DMGEXP is a specific parameter. Parameter DCRIT defines the minimum damage that must accumulate to couple the stress tensor with damage.

$$\sigma = \bar{\sigma} \cdot \left[1 - \left(\frac{D - DCRIT}{1 - DCRIT}\right)^{\mathrm{FADEXP}}\right] \tag{8}$$

$DCRIT$ is the critical damage when instability parameter $F = 1$.

The instability parameter defines the initial state of the failure process. Once the critical value is reached, the structure is likely to fail under the prescribed load.

$$F = \left(\frac{\varepsilon}{\varepsilon_{crit}(\eta)}\right)^{\mathrm{DMGEXP}} \tag{9}$$

where $\varepsilon_{crit}(\eta)$ is the equivalent plastic strain to initiate the instability process.

The strain to failure ε_f is determined from experimental data. For this purpose, samples were prepared for DIC analysis and subsequently subjected to tensile loading (Figure 11).

Results reveal that a strain at failure (ε_f) at least 0.5 is reached. For this analysis only bone-shaped samples were used. Therefore, the triaxiality curve is defined to capture the effect for uniaxial loading.

$$\begin{aligned} \varepsilon_{f,\eta=0.00} &= 1.00 \\ \varepsilon_{f,\eta=0.33} &= 0.50 \\ \varepsilon_{f,\eta=1.00} &= 1.00 \end{aligned} \tag{10}$$

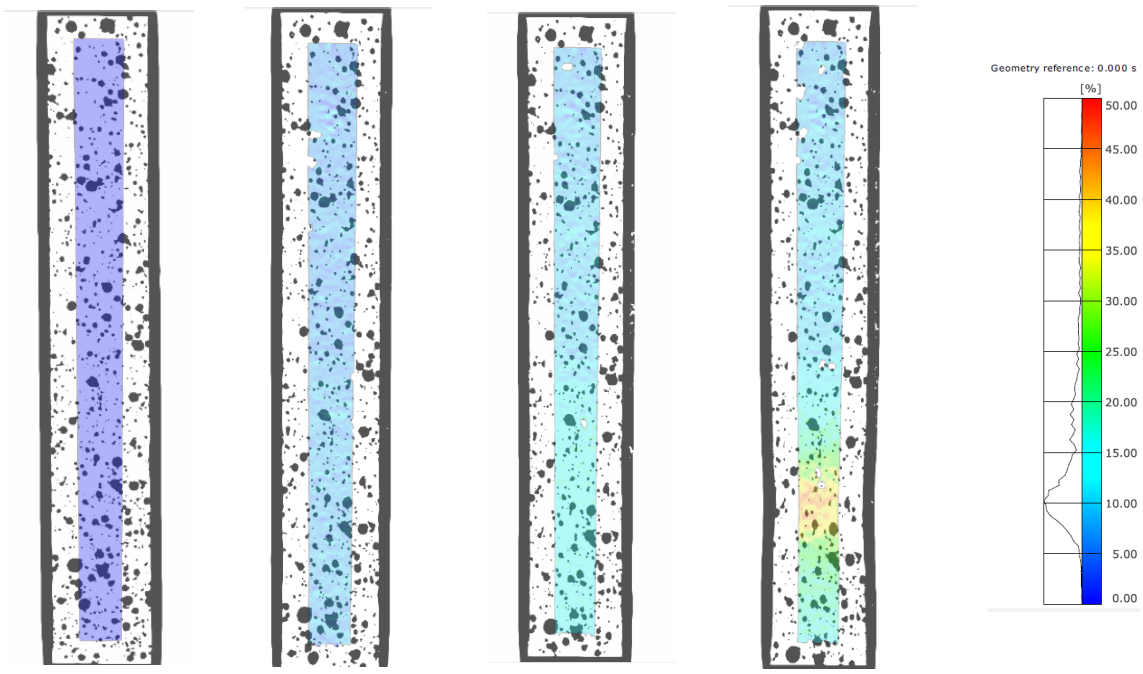

Figure 11. Results from DIC analysis

Figure 12 presents the simulation result obtained using the material model with damage.

a)

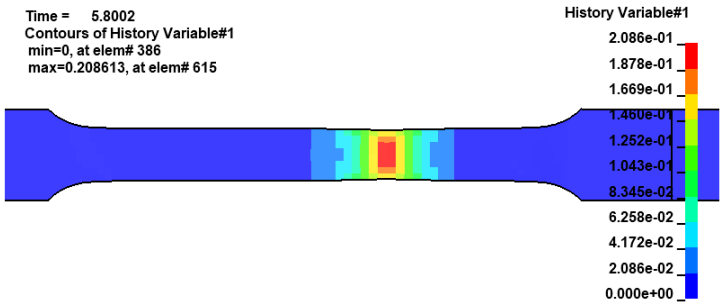

b)

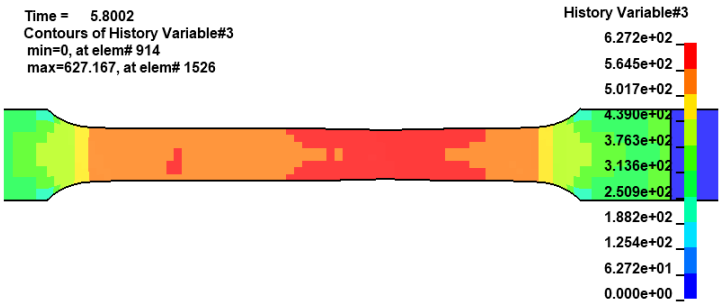

c)

Figure 12. Simulation results: *a)* instability parameter; *b)* damage parameter; *c)* stress

The parameters DMGEXP and FADEXP are determined by an iterative process (Figure 13).

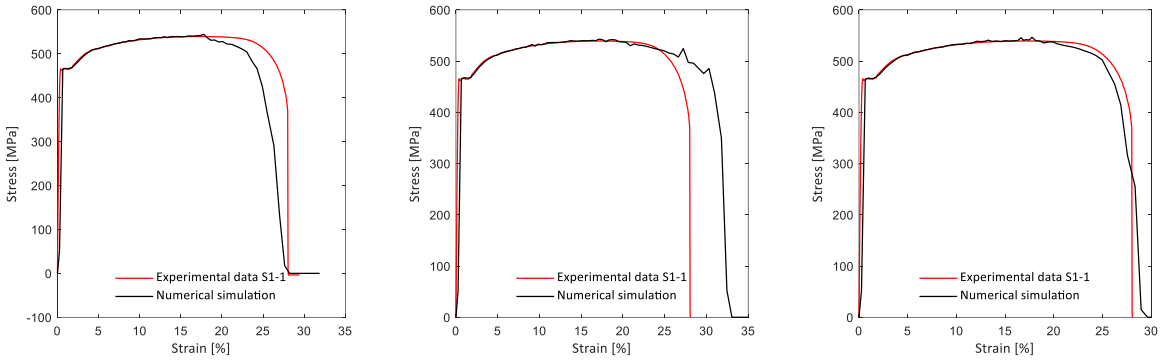

$DMGEXP = 1.2$
$FADEXP = 1.5$
$ECRIT = 0.15$

$DMGEXP = 1.5$
$FADEXP = 1.41$
$ECRIT = 0.15$

$DMGEXP = 1.5$
$FADEXP = 1.42$
$ECRIT = 0.15$

Figure 13. Parameter calibration

Figure 14 presents the stress evolution in the necking section showing the global stress state, stress localization, pre-fracture and post-fracture.

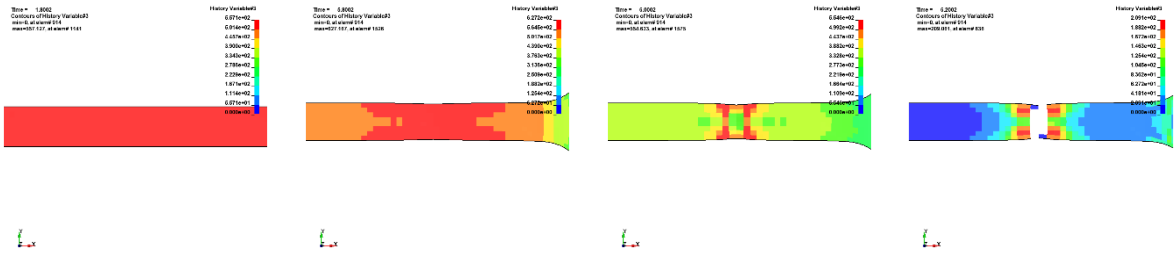

Figure 14. Stress evolution

CONCLUSIONS

The paper addresses the process of identifying the mechanical properties of S460 steel. The engineering data, recorded from the tensile tests, are discussed to determine the relevance of the results.

Subsequently these data are converted to true stress-strain data which are relevant to the design process.

A material model is developed for numerical simulation. Thus, a virtual sample is tested in traction to determine the stress response. Results are in perfect agreement with experiments.

To extend the capability of material the damage model available for numerical simulation was implemented. The data acquisition process and the model calibration are briefly discussed.

The material complies with general prescriptions and the numerical model is reliable for simulations.

REFERENCES

[1] H. Fransplass, M. Langseth, O.S. Hopperstad, Numerical study of the tensile behaviour of threaded steel fasteners at elevated rates of strain, Int J Impact Eng 54 (2013) 19–30. https://doi.org/10.1016/j.ijimpeng.2012.10.009.

[2] S. Ereiz, I. Duvnjak, J. Fernando Jiménez-Alonso, Review of finite element model updating methods for structural applications, Structures 41 (2022) 684–723. https://doi.org/10.1016/j.istruc.2022.05.041.

[3] E. Wang, R. Yao, Q. Li, X. Hu, G. Sun, Lightweight metallic cellular materials: A systematic review on mechanical characteristics and engineering applications, Int J Mech Sci 270 (2024). https://doi.org/10.1016/j.ijmecsci.2023.108795.

[4] T. Fadiji, C.J. Coetzee, T.M. Berry, A. Ambaw, U.L. Opara, The efficacy of finite element analysis (FEA) as a design tool for food packaging: A review, Biosyst Eng 174 (2018) 20–40. https://doi.org/10.1016/j.biosystemseng.2018.06.015.

[5] A. Milone, P. Foti, F. Berto, R. Landolfo, Post-necking and damage modelling of steel structural components: A comprehensive state of the art, Eng Struct 321 (2024). https://doi.org/10.1016/j.engstruct.2024.118931.

[6] L. Yi, Z. Gu, G. Yu, X. Li, Z. Tang, Y. Zhao, Damage behavior and performance analysis of Al5083 alloy in superplastic bulging, Eng Fail Anal 164 (2024). https://doi.org/10.1016/j.engfailanal.2024.108732.
[7] Y. Duan, X. Zhuang, H. Ren, T. Rabczuk, An open-source LS-DYNA implementation of the variational damage model, Advances in Engineering Software 206 (2025). https://doi.org/10.1016/j.advengsoft.2025.103924.
[8] G. Cui, X. Zhai, L. Meng, Behavior of axially loaded high-strength steel circular hollow section tubes under low velocity lateral impact, Thin-Walled Structures 185 (2023). https://doi.org/10.1016/j.tws.2023.110595.
[9] Test Methods for Tension Testing of Metallic Materials, (2013). https://doi.org/10.1520/E0008_E0008M-13A.
[10] N. Wawrzyniak, P. Wanjara, M. Brochu, M. Brochu, Measuring the tensile properties of Ti6Al4V fabricated by laser powder bed fusion: Influence of specimen dimensions, Theoretical and Applied Fracture Mechanics 131 (2024). https://doi.org/10.1016/j.tafmec.2024.104419.
[11] C. Hoffarth, S.D. Rajan, R.K. Goldberg, D. Revilock, K.S. Carney, P. DuBois, G. Blankenhorn, Implementation and validation of a three-dimensional plasticity-based deformation model for orthotropic composites, Compos Part A Appl Sci Manuf 91 (2016) 336–350. https://doi.org/10.1016/j.compositesa.2016.10.024.
[12] M. Güden, H.İ. Erten, R.M. Gorguluarslan, U.C. Gülletutan, A. Dağkolu, İ. Gökdağ, A.C. Gunaydın, S. Altınok, H.İ. Erol, S. Namazov, A comprehensive study on the effectiveness of the stress and damage model parameters in predicting the compression fracture behavior of Selective Laser Melted AlSi10Mg BCC lattices, Mechanics of Materials (2025) 105395. https://doi.org/10.1016/j.mechmat.2025.105395.
[13] N.Y. Kim, N.H. Kim, M.K. Razali, H.M. Lee, M.S. Joun, Analytical and numerical evaluation of the relationship between elongation calibration function and cyber standard tensile tests for ductile materials, Mater Des 253 (2025). https://doi.org/10.1016/j.matdes.2025.113851.
[14] M. Vogler, S. Kolling, A. Haufe, A Constitutive Model for Plastics with Piecewise Linear Yield Surface and Damage, 2007.
[15] S. Jayakumar, A. Hajdarevic, S. Anand, X. Fang, Experimental and FE analyses of the crushing and bending behaviors of GMT and hybrid-formed Al-GMT structures, Thin-Walled Structures 186 (2023). https://doi.org/10.1016/j.tws.2023.110648.
[16] N. Novak, L. Starčevič, M. Vesenjak, Z. Ren, Blast response study of the sandwich composite panels with 3D chiral auxetic core, Compos Struct 210 (2019) 167–178. https://doi.org/10.1016/j.compstruct.2018.11.050.
[17] N. Novak, L. Starčevič, M. Vesenjak, Z. Ren, Blast response study of the sandwich composite panels with 3D chiral auxetic core, Compos Struct 210 (2019) 167–178. https://doi.org/10.1016/j.compstruct.2018.11.050.
[18] G. Gu, Y. Xia, Q. Zhou, On the fracture possibility of thin-walled tubes under axial crushing, Thin-Walled Structures 55 (2012) 85–95. https://doi.org/10.1016/j.tws.2012.03.005.
[19] M. Kõrgesaar, The effect of low stress triaxialities and deformation paths on ductile fracture simulations of large shell structures, Marine Structures 63 (2019) 45–64. https://doi.org/10.1016/j.marstruc.2018.08.004.
[20] M. Dai, L. Ying, S. Wang, H. Ma, P. Hu, Y. Wang, Modeling the crashworthiness analysis of functional graded strength thin-walled structure with phenomenological GISSMO model, Thin-Walled Structures 180 (2022) 109766. https://doi.org/10.1016/j.tws.2022.109766.